Modeling of the N_2$^+$ ion in cold helium plasma II: transport properties of N_2$^+$ in helium

Stanilas Paláček, Martin Beseda, René Kalus, Malika Benhenni, Florent X. Gadéa, Thierry Leininger, Mohammed Yousfi

Modeling of the N_2^+ ion in cold helium plasma II: transport properties of N_2^+ in helium.

S Paláček[1,2], M Beseda[1], R Kalus[1,2], M Benhenni[3], F X Gadéa[4], T Leininger[4], and M Yousfi[3]

[1] IT4Innovations National Supercomputing Center, VŠB–Technical University of Ostrava, 17. listopadu 2172/15, 708 00 Ostrava–Poruba, Czech Republic

[2] Department of Applied Mathematics, Faculty of Electrical Engineering and Computer Science, VŠB–Technical University of Ostrava, 17. listopadu 2172/15, 708 00 Ostrava–Poruba, Czech Republic

[3] Laboratoire Plasma et Conversion d'Energie, LAPLACE & UMR5213 du CNRS, Université de Toulouse III Paul Sabatier, 118 route de Narbonne, 31062 Toulouse Cedex, France

[4] Laboratoire de Chimie et de Physique Quantiques, IRSAMC & UMR5626 du CNRS, Université Toulouse III – Paul Sabatier, 31062 Toulouse Cedex 09, France

E-mail: martin.beseda@vsb.cz, stanislav.palacek@vsb.cz, rene.kalus@vsb.cz, gadea@irsamc.ups-tlse.fr, thierry.leininger@irsamc.ups-tlse.fr, malika.benhenni@laplace.univ-tlse.fr

Abstract. A detailed modeling of N_2^+ transport properties in helium gas has been performed by employing Monte Carlo calculations based on *ab initio* collision cross-sections reported by our group in a preceding paper (Ref. [1]). A broad range of the reduced electric field (E/N) is considered to provide data directly usable in macroscopic modeling of processes in cold helium plasmas. The N_2^+ mobility in helium gas at room temperature ($T = 300\,\mathrm{K}$), the characteristic energies of its longitudinal and transversal diffusion, and the rate constant of the N_2^+ dissociation induced by collisions with helium atoms have been calculated. The effect of the N_2^+ initial rotational-vibrational excitation is investigated as well as the effect of the rotational alignment of the N_2^+ molecule. A direct comparison with N_2^+/He mobility experimental data is performed as well as indirect tests of theoretical estimates of the characteristic diffusion energies by comparing the latter with pseudo-experimental data obtained from mobility experiments via an inverse-method approach.

1. Introduction

In a preceding paper [1], we have reported *ab inito* cross-sections of the most important processes resulting from collisions of N_2^+ ions with helium gas, the *non-reactive scattering* (NRS) process,

$$N_2^+ + He \rightarrow N_2^+ + He, \tag{1}$$

and the *collision-induced dissociation* (CID) of the N_2^+ ion,

$$N_2^+ + He \rightarrow N^+ + N + He. \tag{2}$$

In the present paper, we further develop the investigation by extending the performed calculations to the transport properties of the N_2^+ ion in helium gas and the rate constant of the CID of the N_2^+ ion. Importantly, state-of-the-art experimental data [2, 3, 4, 5] are available in the literature for the N_2^+/He mobility and, as a consequence, a direct assessment of the reliability of our simulation approaches is feasible. For the other quantities, there are, to our best knowledge, no measurements reported in the literature and the predictions we have calculated within the present work may partly fill this gap.

In the calculations reported below, an optimized Monte Carlo (MC) code [6] has been used with the previously calculated cross-sections employed as independent inputs. The room temperature ($T = 300\,\mathrm{K}$) and a broad range of the external electric field have been considered to reproduce typical experimental conditions. As discussed before [1], the main motivation of this work consists, in general, in the modeling of interactions and processes in cold (room-temperature) helium plasma, particularly the interactions of the plasma with environment (air) after the plasma leaves the inner space of a generator. An ultimate goal of this broader research aim is to provide realistic input data for macroscopic modelings of cold helium plasmas needed to optimize their use in various, mainly biomedical applications [7, 8, 9]. In this sense, the present paper represents a topmost level of the work leading to data ready to use in such macroscopic modelings.

To briefly summarize the preceding cross-section calculations (for details see Ref. [1]), a direct dynamics approach [10] was applied to the N_2^+/He collisions with related

calculations performed on the electronic ground-state potential energy surface of the collision complex and by treating atomic nuclei classically. The interaction energy and forces have been calculated on-the-fly using standard *ab initio* methods[1]. In the preceding paper [1], the *multi-configuration self-consistent field* (MCSCF) method [11, 12] was used, as implemented in the MOLPRO suite of *ab initio* codes [13], versions *mpp-2020.1.2* and *mpp-2021.1*. The method represents an acceptable trade-off between accuracy and computational demands [14]. A quasi-classical trajectory (QCT) method [15] was employed to integrate bunches of classical trajectories which were subsequently used to calculate collision cross-sections of the NRS and CID processes.

The course of the present paper is organized as follows. First, a short summary of the methods employed in calculations is provided in Sec. 2. Only the methods directly related to the present work are discussed, for further information about the dynamical calculations leading to the collision cross-sections see Ref. [1]. The main part of the present paper, Sec. 3, presents and discusses the most important results we have obtained. We start with a thorough comparison of our theoretical results with available experimental data in Subsec. 3.1 and continue with a detailed discussion of the effect of the initial rotational-vibrational excitation and the rotational alignment [16] of the N_2^+ ion on its transport properties (mobility and diffusion) and dissociation rate in Subsecs. 3.2 and 3.3, respectively. Finally, conclusive remarks are provided in Sec. 4.

2. Methods and computations

The transport coefficients and the CID rates of the N_2^+ ion have been calculated using an optimized Monte Carlo method as introduced and described in detail in Ref. [6]. Briefly, the method is based on propagating a large number of ionic seeds through the carrier gas under the action of a uniform electric field and simulating a correspondingly large number of ion–neutral collisions, one by one, with collision probability obtained from pre-calculated collision cross-sections. Ion–ion collisions are neglected since the concentration of carrier gas atoms is expected to considerably exceed the concentration of ions. For each simulated collision, the probabilities of NRS and CID reaction channels are as well evaluated from the pre-calculated cross-sections.

In the Monte Carlo simulations, initial parameters, like the maximum collision time ($t_{\max}$), maximum ion energy ($E_{\max}$) and the number of ionic seeds (N_{seed}), are adjusted until a hydrodynamic equilibrium (steady state) is reached. It occurs when the mean ion velocity reaches, as a function of time, a plateau and when a good level of convergence is obtained for the ion energy distribution, transport coefficients, and reaction rate constants. For example, for a reduced field of $E/N = 10\,\text{Td}$, the following values have been used: $t_{\max} = 4\,\mu\text{s}$, $E_{\max} = 0.4\,\text{eV}$, and $N_{\text{seed}} = 2 \times 10^6$. The total number of simulated collisions, including the fictitious ones [6], has been about 57×10^6

1 In some specific cases, computationally cheaper representations of *ab initio* data through artificial neural networks (ANNs) were used to save computer time. See Subsec. 3.3 for more details.

in this case.

Typical relative errors obtained in the Monte Carlo simulations depend on particular values of sampling parameters and on the type of calculated coefficients (see also Ref. [17]). The errors are lowest for the mean ion energy (since all the directions of ion drift are considered), intermediate for the ion reduced mobility (because only the velocity along the electric field axis is sampled), and the relative errors become rather large when the variance of the ion position along a given direction is considered (like in calculations of the characteristic diffusion energies, see below). In the case of the ion mobility, the relative errors are around 0.1 % and 0.02 % at $E/N = 10\,\mathrm{Td}$ and $E/N = 500\,\mathrm{Td}$, respectively, whereas typical relative errors obtained for characteristic diffusion energies are at least an order of magnitude larger (1 % and 0.5 %, respectively).

Standard formulas have been used to calculate required quantities from microscopic data collected along the Monte Carlo simulations: the reduced mobility ($K_0 N$) of the N_2^+ ion in helium gas at standard pressure ($P_0 = 760\,\mathrm{torr}$) and temperature ($T_0 = 273.16\,\mathrm{K}$),

$$K_0 N = \frac{\langle v_z \rangle}{(E/N)} \frac{T_0}{T_{\mathrm{gas}}} \frac{P_{\mathrm{gas}}}{P_0}, \tag{3}$$

coefficients of longitudinal (D_{L}) and transversal (D_{T}) diffusion of N_2^+ ions through the carrier gas,

$$D_{\mathrm{L}} = \frac{1}{2} \frac{\mathrm{d}\left[z(t) - \langle z \rangle\right]^2}{\mathrm{d}t}, \tag{4}$$

$$D_{\mathrm{T}} = \frac{1}{4} \frac{\mathrm{d}\left\{\left[x(t) - \langle x \rangle\right]^2 + \left[y(t) - \langle y \rangle\right]^2\right\}}{\mathrm{d}t}, \tag{5}$$

and the reaction rate constant of the CID of the N_2^+ ion,

$$k_{\mathrm{CID}} = \frac{\langle \nu_{\mathrm{CID}} \rangle \, \nu_{\mathrm{tot}}}{N}. \tag{6}$$

In all the formulas, the electric field is assumed to be oriented along the z axis and the symbols used are as follows: T_{gas} and P_{gas} are respectively the temperature and pressure of the carrier gas, x, y, z stand for coordinates and v_x, v_y, v_z for velocity components of the migrating ion, ν_{tot} is the total collision frequency, $\langle \nu_{\mathrm{CID}} \rangle$ is the average frequency of collisions leading to the CID of the N_2^+ ion, and N is particle density of the carrier gas. The averages, denoted by brackets in Eqs. (3)–(6), are calculated as

$$\langle X \rangle = \frac{1}{n_{\mathrm{p}}} \sum_{i=1}^{n_{\mathrm{p}}} \frac{1}{n_{\mathrm{c}}} \sum_{j=1}^{n_{\mathrm{c}}} X_{ij}, \tag{7}$$

with n_{p} being the number of seed N_2^+ particles, n_{c} representing the total number of recorded N_2^+ collisions, and X_{ij} being the value of quantity X of seed i in collision j.

As discussed in a more detailed way in Ref. [1], two types of integral cross-sections calculated at the momentum-transfer approximation level [18], momentum-transfer cross-sections (MTCSs), have been calculated for the NRS process,

$$\sigma_{\mathrm{NRS}}^{(\mathrm{MT1})} = \int_{4\pi} \left[\frac{\mathrm{d}\sigma}{\mathrm{d}\Omega}\right]_{\mathrm{NRS}} (1 - \cos\theta) \, \mathrm{d}\Omega, \tag{8}$$

$$\sigma_{\mathrm{NRS}}^{(\mathrm{MT2})} = \int_{4\pi} \left[\frac{\mathrm{d}\sigma}{\mathrm{d}\Omega}\right]_{\mathrm{NRS}} \left(1 - \frac{p'}{p}\cos\theta\right) \mathrm{d}\Omega, \tag{9}$$

where $[\mathrm{d}\sigma/\mathrm{d}\Omega]_{\mathrm{NRS}}$ is the differential cross-section of the NRS process, $\mathrm{d}\Omega$ stands for an element of solid angle, θ is the scattering angle, and p and p' denote the magnitudes of linear momentum of the He atom before and after collision, respectively. Note that the type 1 MTCS, Eq. (8), was originally introduced for elastic scattering processes of structure-less particles [18] while the type 2 MTCS, Eq. (9), was proposed [19] for a presumably more realistic description of inherently inelastic collisions accompanied by energy transfer between translational and internal degrees of freedom of colliding particles. Nevertheless, as shown in Ref. [1], the differences between the two types of MTCSs are only marginal for N_2^+/He collisions. As a consequence, the type 1 MTCSs have been mainly reported in Ref. [1] and are used in the present Monte Carlo calculations. For the CID process, the standard integral cross-section has been considered[2],

$$\sigma_{\mathrm{CID}}^{(\mathrm{int})} = \int_{4\pi} \left[\frac{\mathrm{d}\sigma}{\mathrm{d}\Omega}\right]_{\mathrm{CID}} \mathrm{d}\Omega. \tag{10}$$

In addition to cross-sections obtained from dynamical calculations, another set of type 1 MTCSs have been calculated using a so-called *inverse method* (IM) approach [20]. The procedure adopted in our calculations has been in detail described in Ref. [1] and only a short summary is thus needed here. A simple isotropic interaction potential has been adjusted against available experimental N_2^+/He mobility data in an iterative procedure comprising a) the potential adjustment, b) cross-sections calculations via a semiclassical JWKB method [21], and c) a Monte Carlo calculation of the N_2^+/He mobility. The calculations are repeated until a sufficiently good correspondence is achieved between calculated and measured mobilities. In this way, resulting IM-derived cross-sections can be subsequently used in calculations of other quantities, e.g., the diffusion coefficients, and provide pseudo-experimental estimates of these quantities where measurements are not available. Since the CID process is excluded from the IM treatment, such a procedure cannot be, on the other hand, employed for getting a pseudo-experimental estimate of the N_2^+ CID cross-sections and dissociation rate constants.

2 The usual integral cross-section cannot be used for the NRS process, since the corresponding differential cross-section has, within the classical approach used in this work, a non-integrable singularity as θ approaches 0 and the corresponding integral cross-section thus diverges. The cosine terms in Eqs. (8) and (9) remove this divergence at the expense of introducing only marginal errors. Nothing like that occurs, however, for the CID due to the existence of a rather high energetic threshold of the latter reaction.

3. Results and discussions

3.1. Comparison with experiments

A comparison with experimental data is generally considered the ultimate test of validity of used theoretical approaches and, as such, is an obligatory part of any theoretical study whenever such a comparison is feasible. For the N_2^+ ion in helium carrier gas, a couple of precise measurements exist on its mobility and a direct comparison with calculated estimates is thus possible. For the other quantities considered in the present work (coefficients of the longitudinal and transversal diffusion of N_2^+ in helium and its dissociation rate), on the other hand and to our best knowledge, no such direct measurements are available. Nevertheless, as discussed above, an indirect comparison can be made for the diffusion coefficients in terms of pseudo-experimental data calculated through the IM approach. More specifically, the IM momentum-transfer cross-sections of Ref. [1] have been used to calculate the diffusion coefficients through Monte Carlo simulations discussed in Sec. 2 and subsequently compared with numerical data obtained from dynamical calculations.

Selected measurements of the N_2^+/He mobility (K_0N) [2, 3, 4, 5, 22] published in the course of the last five decades are summarized in Fig. 1. Clearly, the more recent ones [2, 3, 4, 5] agree very well with one another and their reliability may thus be considered verified. The oldest measurement [22], however, heavily deviates from the more recent ones and, for this reason, will not be taken into account in the present analysis. For the remaining experimental data, their IM representations have been calculated and are also shown in Fig. 1 for comparison. It is clear that the IM representations of the N_2^+/He mobility data perfectly reproduce the measured points over the whole range of the reduced electric field. Noteworthy, such a perfect correspondence was previously reported for the data of Ref. [2] in another, independent theoretical study [23]. The agreement seen in Fig. 1 may become even more obvious if one realizes that, e.g., an uncertainty up to about 7 % ($\approx \pm 1.4\,\mathrm{cm^2V^{-1}s^{-1}}$ in the low-field plateau region) was predicted [3] for the measurement of Ref. [2] and an error bar of about 1−3 % was reported for the data of Ref. [5]. Considering the expected reliability of the IM estimates and for sake of clarity, only the IM representations will be used in the following analysis.

A comparison of our estimates of transport properties calculated for the rotationally-vibrationally ground-state N_2^+ ion (j=0,v=0) with pseudo-experimental IM benchmarks is performed in Fig. 2. In the upper panel of the figure, the N_2^+/He mobility is considered with the most important observation being that the agreement between our theoretical data and the IM data is very good. This particularly holds for the IM representation of the most recent experimental mobility data of Ref. [5] for which almost perfect coincidence is achieved. But, also for the other experiments considered in Fig. 2, the maximum deviation between theoretical and IM data is not major and always below 5−6 %. Another interesting conclusion one can make is that the good correspondence between the theoretical and IM data probably indicates that either the experimental populations of N_2^+ are only slightly rotationally-vibrationally excited or

that the excitations do not much affect the outputs of mobility measurements. This point will be more thoroughly analyzed in the next subsection. In addition to the IM mobility data, results of an independent theoretical study [24] are also shown in the upper panel of Fig. 2 for comparison. Even though this preceding calculation seems to slightly overestimate both our theoretical as well as experimental points, the overall agreement is again very good. The deviations between our data and the data reported in Ref. [24] are always below 2 %. This seems to cross-validate both calculations.

In the lower panel of Fig. 2, our theoretical and pseudo-experimental IM estimates of the coefficients of longitudinal (D_L) and transversal (D_T) diffusion of the N_2^+ ion in helium are compared. Note that only the IM values obtained from cross-sections derived from the most recent experimental mobility data of Ref. [5] are shown for simplicity since the two remaining IM data based on the experiments of Refs. [2, 4] almost coincide with the depicted one. Like for the N_2^+ mobility, a perfect agreement is seen between theoretical and pseudo-experimental IM data for weak and medium electric fields. This holds for both D_L and D_T, with the upper limits of E/N below which the agreement is quantitative being $E/N \approx 100\,\mathrm{Td}$ and $E/N \approx 300\,\mathrm{Td}$, respectively. Only above these strong-field limits, noticeable deviations are seen for D_L and to much less extent also for D_T.[3] This roughly corresponds to the E/N region in which the theoretical values of the N_2^+ mobility also visibly deviate from the IM ones, though much less apparently. It seems that the diffusion coefficients, D_L in particular, are much more sensitive to the differences between theoretical and IM N_2^+/He collision cross-sections seen at higher collision energies, $E_\mathrm{coll} \gtrsim 2\,\mathrm{eV}$ (see Fig. 2 of Ref. [1]).

At the end of this subsection, let us analyze and discuss the almost perfect agreement obtained between experimental (IM) and theoretical values of the N_2^+/He mobility and diffusion coefficients. Particularly, for the most recent experimental mobility data [5], we have found [1] that resulting IM cross-sections (MTCSs) agree very well with our theoretical estimates only over a limited range of collision energies (ranging between $E_\mathrm{coll} \approx 0.05\,\mathrm{eV}$ and $E_\mathrm{coll} \approx 2\,\mathrm{eV}$). Outside this region, the agreement is much worse with the differences between the theoretical and IM data being well apparent. For the mobility data, on the other hand, a very good agreement is seen over almost the whole range of the reduced electric field considered in Fig. 2, at least up to $E/N \approx 200$–$250\,\mathrm{Td}$.

The roots of this seeming discrepancy may be revealed from Fig. 3 where distributions of the center-of-mass N_2^+/He collision energy are depicted for selected values of the reduced electric field. These distributions reach their maxima around $E_\mathrm{coll} \approx 0.04\,\mathrm{eV}$ for $E/N = 10\,\mathrm{Td}$ and around $E_\mathrm{coll} \approx 1.9\,\mathrm{eV}$ for $E/N = 100\,\mathrm{Td}$. It means that typical collision energies at which the N_2^+/He collision takes place in electric fields for which the perfect agreement is seen between theoretical and experimental N_2^+ mobility values fall into the region where a similarly good agreement is seen for cross-sections. On the other hand, for $E/N = 500\,\mathrm{Td}$ (where a well visible difference is seen

3 Note also that, for D_T, the deviations between theoretical and IM values fall inside the estimated error bar of the IM data even for the highest value of E/N.

between IM and theoretical N_2^+/He mobility data), the corresponding maximum of the collision energy distribution lies at $E_{\rm coll} \approx 20\,{\rm eV}$, a value which belongs to the $E_{\rm coll}$ region where a non-negligible discrepancy is seen between IM and theoretical N_2^+/He collision cross-sections.

3.2. The effect of N_2^+ *rotational-vibrational excitations*

In the upper panel of Fig. 4, the dependence of the N_2^+ mobility on the ion rotational-vibrational excitation is analyzed. In general, a moderate effect is observed with the data calculated for rotationally and/or vibrationally excited N_2^+ ions deviating only slightly from the ground-state (j=0,v=0) data. Deviations not larger than about $\pm 1.2\,{\rm cm^2V^{-1}s^{-1}}$ are obtained, which represents about 5 % in the weak-field region and 12 % for strong reduced electric fields. Further, a decrease in the N_2^+ mobility values is induced by both rotational and vibrational excitations in the ion in the weak-field region while a slight enhancement is seen in strong electric fields for vibrational excitations and almost zero effect for rotational excitations of the ion. In weak fields, the rotational excitation of the N_2^+ ion seems to affect its mobility more efficiently than vibrational excitations while the latter seems, on the other hand, to be more efficient in strong fields.

This is in good agreement with an observation made in Ref. [1], namely that the rotational and/or vibrational excitation increases the N_2^+/He MTCSs at low collision energies while the MTCSs are decreased for vibrationally excited ions at high collision energies and remains basically unchanged if the ions are rotationally excited. The former is rather easily understood since both rotational and vibrational excitations are expected to increase the effective geometric cross-section of the N_2^+ ion which, in the weak-field region where the collisions are almost thermal (isotropic), leads to a decrease of the ion mobility simply because the overall resistance of the carrier gas must increase if the ions become "bigger". The observed behavior in the strong field region is, on the other hand, somewhat less intuitive.

Under such conditions, high-energy, strongly anisotropic collisions take place between N_2^+ ions and the helium buffer gas with the ions velocity dominantly aligned along the direction of the applied electric field. Moreover, almost head-on collisions with the buffer gas atoms contribute, as manifested by a dramatic decrease of the effective collision cross-section as the collision energy grows up, during which a massive energy flow occurs between the ions and the buffer gas. In such collisions, the N_2^+ ions are decelerated and their mobility significantly drops, as seen in both calculations and experiments. However, it seems to follow from the inset of the upper panel of Fig. 4 that this deceleration is less efficient for the rotationally and/or vibrationally excited ions than for the ground-state (j=0,v=0) ones. Energy flow between the translational degrees of freedom of the N_2^+/He complex and internal degrees of freedom of the N_2^+ ion may offer a plausible explanation. Moreover, the statistical uncertainty of the mobility data as obtained from Monte Carlo simulations is estimated to be $\lesssim 0.1$ % and the error

introduced by the momentum-transfer approximation should not exceed 2 % [17]. Since both errors are well below the observed effect, it is improbable that the effect is caused only by computational uncertainties.

Indeed, preliminary calculations [25] performed for rotationally excited N_2^+ ions (j=36,v=0) show that the probability of their additional, collision-induced excitation is almost the same as the probability of their deexcitation. On the average, the collisions are close to elastic. For the ground-state ion (j=0,v=0), on the other hand, only rotational excitations are allowed. This means that a transfer of the collision energy to the internal degrees of freedom of N_2^+ takes place and this finally leads to relatively more efficient deceleration of the ground-state ion as compared with rotationally excited ions. Since, as follows from the preliminary calculations, rather high excitations can be achieved at high collision energies in the former case (up to $j \approx 100$ for $E_{\rm coll} = 5\,{\rm eV}$), the resulting additional deceleration of the ground-state ion may become well observable. It seems thus that the difference between the mobility of rotationally excited N_2^+ ions (j=36,v=0) and the mobility of the ground-state ion observed at $E/N \to 0$ will be reduced if the strength of the electric field grows up.

A similar comparison of the N_2^+ in He diffusion coefficients is made in the middle panel of Fig. 4. Clearly, the effect of the N_2^+ rotational and/or vibrational excitation is better seen, for both longitudinal and transversal diffusion, in the strong-field region, particularly for vibrationally excited N_2^+, while almost no change with respect to the j=0,v=0 data is basically observed in weak electric fields. However, even if visible, the changes are only moderate. For example, a change between -11 % and $+4$ % (-7 % and $+1$ %) is seen for the longitudinal (transversal) coefficient for j=0,v=1 and about the same relative change is seen for j=0,v=10, just with opposite signs. The rotational excitation of the N_2^+ ion (j=36,v=0) leads to even slightly smaller deviations not exceeding, for both diffusion coefficients, ± 5 %.

The effect of rotational and vibrational excitations in the N_2^+ ion on the rate of its CID is visualized in the bottom panel of Fig. 4. Here, as more or less expected, a significant change in the CID rate constant ($k_{\rm CID}$) is observed as the excitation energy pumped to the ion grows up (regardless of whether rotational or vibrational degrees of freedom have been excited). For example, while an increase of about 3 times is seen for j=36,v=0 and j=0,v=1 (about $+0.3\,{\rm eV}$ above the ground state, j=0,v=0, at the level of theory used for cross-section calculations [1]) at $E/N = 500\,{\rm Td}$, a two orders of magnitude jump of $k_{\rm CID}$ takes place for this strong field if j=0,v=10 ($+2.5\,{\rm eV}$) is considered. Moreover, a considerable shift of the $k_{\rm CID}$ threshold towards $E/N \to 0\,{\rm Td}$ is also clear as the internal excitation of the N_2^+ ion grows up. Basically, the effect of N_2^+ rotational-vibrational excitations on the ion CID is much stronger than observed in the case of N_2^+ transport properties.

To illustrate expected uncertainties of transport data due to the use of either type 1 or type 2 MTCSs (Eqs. (8) and (9), respectively), differences in the N_2^+ mobility calculated using the two types of MTCS are depicted in Fig. 5. A similar conclusion follows from this figure like that made for cross-sections [1], the differences are mostly

insignificant (up to 1 %) for all the N_2^+ rotational and vibrational excitations considered and over the whole range of the reduced electric field. This is particularly clear for vibrational excitations of the N_2^+ ion for which the differences are well inside a ± 1 % limit (or even much smaller as $E/N \to 0$). Even though the differences seen for the rotationally excited ion (j=36,v=0) are much better pronounced (up to about $0.6\,\mathrm{cm^2V^{-1}s^{-1}}$ at $E/N = 1\,\mathrm{Td}$), the corresponding relative deviation (2.4 %) is still rather small. For example, this value is more than two times smaller than the difference between the j=36,v=0 and j=0,v=0 data.

3.3. The effect of N_2^+ *angular momentum alignment*

In Ref. [1], the effect of N_2^+ angular momentum alignment on calculated cross-sections has been studied, to save computer time, using artificial neural network (ANN) representations of the N_2^+/He potential energy surface. Specifically, separate ANNs have been trained for each particular choice of the N_2^+/He collision energy and N_2^+ rotational-vibrational excitation by employing *ab initio* (MCSCF) energies calculated on the fly in the course of dynamical calculations. In this way, highly accurate ANNs have been obtained which closely reproduced (almost always within an error limit of several meV) relevant parts of the N_2^+/He potential energy surface as well as calculated cross-sections (see Subec. 3.4 of Ref. [1]). Here, the ANN-based cross-sections of Ref. [1] are used to calculate transport properties of the N_2^+ ion in helium for different alignments of the ion angular momentum.

Prior to discussing these additional calculations, the accuracy of the developed ANNs is tested by comparing the values of the N_2^+/He mobility calculated using cross-sections obtained from dynamical calculations with the *ab initio* (MCSCF) methods employed on the fly with mobility data obtained from the ANNs-based cross-sections. This comparison is made for a specific case of the rotationally-vibrationally ground-state N_2^+ ion (j=0,v=0) in Fig. 6. As is clear from this figure, the mobility data calculated from the "on-the-fly" cross-sections and those obtained from cross-sections calculated using ANN representations of the N_2^+/He potential energy surface match very well each other with relative deviations being always below 1 %. Such a conclusion is not, however, surprising since a similarly favorable picture was already obtained for cross-sections [1].

A comparison of calculations performed with the N_2^+ angular momentum (J) prior to a collision aligned parallel (PAR) with or perpendicular (PER) to the collision axis, and non-aligned (NA) is presented in Fig. 7. The effect of the J alignment is analyzed separately for N_2^+ mobility, diffusion coefficients, and the CID rate constant. Following the preceding cross-section calculations [1], the rotational-vibrational ground state of the N_2^+ ion is considered. Since the angular momentum of the N_2^+ ion is zero for the rotational ground state of the ion, the alignment has been modeled, like in Ref. [1], by specifically aligning the N_2^+ ion in space. For the ion with its center of mass put to the origin of coordinates and the incoming He atom placed in the xz plane and with its velocity oriented along the z axis, the PER alignment of J has been modeled by putting

the ion in a randomly oriented plane going through the z-axis while the PAR orientation of J is represented by the ion placed in the xy plane. In both cases, random orientation of the ion axis in the respective plane is considered. The NA orientations of the ion axis are then randomly generated from an isotropic distribution in space.

For the N_2^+ mobility in He (the upper panel of Fig. 7), the effect of the J alignment is well observable, though far from dramatic. The values obtained for the PER alignment of J are by at most 8 % above the NA values and the values resulting from the PAR alignment are by about the same (relative) deviation decreased with respect to the NA values.

A somewhat better-pronounced PER/PAR/NA differences are seen on the D_L/D_T curves depicted in the middle panel of Fig. 7. While a marginal difference (up to 1 %) is obtained in the weak-field region ($E/N \approx 1$–10 Td), it gradually grows up as the electric field intensity increases. More specifically, for the PER alignment, the deviations of both D_L and D_T from NA values are positive and monotonically rise with E/N up to respectively 25 % or 11 % at $E/N = 500$ Td. In the case of the PAR alignment, quantitatively similar behavior is seen, just the PAR values of both diffusion coefficients are below the NA values.[4]

Finally, the reaction rate constants of the CID of the N_2^+ ion (k_{CID}) calculated for the PER, PAR, and NA alignments of the ion are compared in the bottom panel of Fig. 7, from which it is clearly seen that, in the specific case of the N_2^+ CID, the effect of its alignment is rather strong. The CID rate constant is decreased by at least 85 % for the PAR alignment with respect to NA and increased by 30–80 % for the PER alignment. This is, however, mainly because of the small magnitude of k_{CID} in the specific case of N_2^+/He collisions, absolute deviations are much less dramatic. Somewhat surprisingly, the PER alignment enhances k_{CID} and the PAR alignment leads to decreased values of k_{CID}, despite the fact that reverse holds for related cross-sections, $\sigma_{CID}^{(int)}$. However, one should realize that the values of k_{CID} are in synergy influenced by both the CID cross-sections and the MTCSs of the NRS process (Eq. (1)). In particular, the latter may heavily influence the distribution of N_2^+/He collision energies and give rise to a quite unexpected behavior of k_{CID}.

4. Conclusions

A series of simulations have been performed using an optimized Monte Carlo code [6] and cross-sections derived from direct dynamics calculations [1] employing previously tested *ab initio* approaches [14]. In this way, transport properties (mobility and longitudinal and transversal diffusion coefficients) of the N_2^+ ion in helium gas and the rate of

4 Note that the PER alignment of the N_2^+ angular momentum leads to increased mobility and a more efficient diffusion of the N_2^+ ion while the reverse holds for the PAR alignment. This is not surprising, however, if one takes into account that the effective geometric cross-section of the N_2^+ ion should be smaller for the PER alignment of its angular momentum than for the PAR alignment. As a consequence, the effect is basically a geometric one. See also the discussion of Subsec. 3.4 of Ref. [1].

dissociation of the ion-induced by collisions with helium atoms have been calculated. To model typical conditions in cold helium plasmas, a room temperature ($T = 300\,\mathrm{K}$) has been assumed for the carrier helium gas and a broad range of the reduced electric field has been considered (E/N = 1–500 Td). As independent inputs to these Monte Carlo simulations, cross-sections calculated in a preceding paper [1] have been used, namely the momentum-transfer cross-sections (Eqs. (8) and (9)) of the non-reactive scattering (NRS) of the N_2^+ ion on helium atoms (Eq. 1) and the integral cross-section (Eq. 10) for the collision-induced dissociation (CID) of the N_2^+ ion (Eq. (2)). A thorough comparison with state-of-the-art experimental data on the N_2^+ mobility in He [2, 3, 4, 5] has been performed, the effect of initial (prior to collision) rotational-vibrational excitations of N_2^+ has been studied, as well as the effect of the alignment [16] of the N_2^+ angular momentum. An independent calculation of the N_2^+ mobility in He [24] has also been considered to cross-validate the reported results.

A very good agreement has been achieved between our mobility calculation and experimental values up to very strong electric fields. Particularly perfect correspondence has been obtained for the most recent experimental data of Ref. [5]. Alike, the independent theoretical data on the N_2^+/He mobility of Ref. [24] agree very well with our estimates. In this way, the methodology applied in the present work as well as the calculations of collision cross-sections performed in Ref. [1] have been validated.

The excellent agreement between theoretical and experimental mobility data has also been discussed from the point of view of the fact that slight discrepancies are seen in the underlying cross-section data in high and low collision energy regions [1] and has been interpreted in terms of typical collision energies of the N_2^+/He collision complex under the conditions considered in the present work. The nice correspondence is partly due to the fact that, for most values of the reduced electric field considered in the present work, the N_2^+/He collision energy mainly falls in a region where calculated cross-sections almost perfectly match pseudo-experimental values derived from the experimental mobility data via the inverse method (IM) approach. Only if the strongest electric fields are considered, very high collision energies are gained by the N_2^+ ion which belong to the region where theoretical and IM cross-sections deviate from each other. Not surprisingly, an onset of visible deviations between theoretical and experimental estimates of the N_2^+ mobility is seen in this strong-field region.

The effect of N_2^+ rotational-vibrational excitations is only moderate for the ion mobility, somewhat better pronounced for the coefficients of longitudinal and transversal diffusion of the N_2^+ ion in helium in the strong-field region (and, interestingly, almost none in weak electric fields), and particularly well seen in the case of the rate of N_2^+ dissociation induced by collisions with He atoms. Specifically, the mobility of N_2^+ is reduced in weak electric fields if rotationally and/or vibrationally excited ions are assumed to enter the collisions while the reverse holds if a strong electric field is applied. The effect of N_2^+ rotational-vibrational excitations on the diffusion coefficients is almost exclusively seen only in the strong-field region and even there it is moderate. The rate constant of the CID of the N_2^+ ion is, on the other hand, rather strongly influenced by

the excitation energy pumped into rotational and/or vibrational degrees of freedom of the ion. As expected, the threshold of the dissociation rate constant is pushed to considerably lower values of the electric field as the internal excitation of the ion increases and, moreover, the efficiency of the dissociation process increases.

Alike, the effect of alignment of the N_2^+ angular momentum (J) is well observable, though not dramatic. As expected from geometric considerations, perpendicularly aligned J leads to an increase in the N_2^+ mobility as well as to an increase in diffusion coefficients while J oriented parallelly considerably lowers both. While the J-alignment effect is better pronounced for the N_2^+ mobility in the weak-field region, the diffusion coefficients are much more strongly influenced by a particularly aligned J in strong electric fields. A strong effect of the N_2^+ J-alignment is seen in the case of the CID of the ion. Interestingly and somewhat surprisingly, the effect is reversed to what has been seen for CID cross-sections. While the CID cross-sections are enhanced for the parallel alignment as compared to the values obtained non-aligned J and lowered for the perpendicular alignment (an effect well understandable on the base of geometric considerations [1]), the reverse holds for the CID rate constant. This is highly probably due to the fact that the rate constant is influenced by both the CID cross-sections and MTCSs of the N_2^+/He NRS, where the latter is decisive for the mobility of the ion and, consequently, for the distribution of N_2^+/He collision energies.

In summary, a detailed theoretical investigation of selected transport properties of the N_2^+ ion in helium gas as well as its collision-induced dissociation has been performed. Still, however, some questions remain open and will require a closer look. Among others, let us mention the most important ones, namely a) the question about the role of excited electronic states and non-adiabatic processes in N_2^+/He collisions and b) how the rotational and/or vibrational excitations are populated in the N_2^+ ions. Both calculations are being currently prepared in our group.

Acknowledgments

Financial support by the Ministry of Education, Youth and Sports of the Czech Republic via the *National Programme of Sustainability II*, as implemented in the *IT4Innovations excellence in science* project (grant no. LQ1602), is frankly acknowledged. The calculations have been by part performed on the *IT4Innovations* supercomputers supported through the *e-INFRA CZ* project (grant no. ID:90140) and made available to us through computational grants OPEN-16-3, OPEN-16-14, OPEN-17-15, OPEN-17-50, DD-20-23, OPEN-20-34, OPEN-21-46, OPEN-22-21 and OPEN-23-12. Last but not least, RK would like to acknowledge partial financial support through the *PRACE-6IP* project, the EU *Horizon 2020 research and innovation programme* (grant No. 823767).

References

[1] S. Paláček, M. Beseda, R. Kalus, M. Benhenni, M. Yousfi, T. Leininger, and F. X. Gadéa. Modeling of the N_2^+ ion in cold helium plasma: dynamics of N_2^+/he collisions and cross-sections. Submitted to Plasma Source Sci. Tech.

[2] M. McFarland, D. L. Albritton, F. C. Fehsenfeld, E. F. Ferguson, and A. L. Schmeltekopf. Flow-drift technique for ion mobility and ion-molecule reaction rate constant measurements. II. positive ion reactions of N^+, O^+, and H_2^+ with O_2 and O^+ with N_2 from thermal to $\approx 2\,\mathrm{eV}$. *J. Chem. Phys.*, 59(12):6620–6628, December 1973.

[3] H. W. Ellis, R. Y. Pai, E. W. McDaniel, E. A. Mason, and L. A. Viehland. Transport properties of gaseous ions over a wide energy range. *At. Data Nucl. Data Tables*, 17(3):177, March 1976.

[4] Y. Kaneko, T. Koizumi, and N. Kobayashi. Mobilities of various ions in non-parent gases; Compilation of the mobility data measured with the injected-ion drift tube mass spectrometer in Tokyo Metropolitan University. *J. Mass. Spec. Soc. Japan*, 26(1):35–52, 1978.

[5] E. B. Anthony, M. J. Bastian, V. M. Bierbaum, and S. R. Leone. Laser probing of rotational-state-dependent velocity distributions of $N_2^+(v'' = 0, j)$ drifted in He. *J. Chem. Phys.*, 112(23):10269, June 2000.

[6] M. Yousfi, A. Hennad, and O. Eichwald. Improved monte carlo method for ion transport in ion-molecule asymmetric systems at high electric fields. *J. Appl. Phys.*, 84(1):107–114, 1998.

[7] M. Laroussi. Low-temperature plasmas for medicine? *IEEE Trans. Plasma Sci.*, 37(6):714, June 2009.

[8] M. Yousfi, N. Merbahi, A. Pathak, and O. Eichwald. Low-temperature plasmas at atmospheric pressure: toward new pharmaceutical treatments in medicine. *Fund. Clin. Pharm.*, 28(2):123, February 2014.

[9] H. Tanaka, K. Ishikawa, M. Mizuno, S. Toyokuni, M. Kajiyama, F. Kikkawa and. H.-R. Metelmann, and M. Hori. State of the art in medical applications using non-thermal atmospheric pressure plasma. *Rev. Mod. Plasma Phys.*, 3(1):1, July 2017.

[10] W. L. Hase, K. Song, and M. S. Gordon. Direct dynamics simulations. *Comp. Sci. Eng.*, 5(4):36–44, July 2003.

[11] H.-J. Werner and P. J. Knowles. A second order multiconfiguration scf procedure with optimum convergence. *J. Chem. Phys.*, 82(11):5053–5063, 1985.

[12] P. J. Knowles and H.-J. Werner. An efficient second-order MC SCF method for long configuration expansions. *Chem. Phys. Lett.*, 115(3):259–267, 1985.

[13] H. J. Werner, P. J. Knowles, F. R. Manby, J. A. Black, K. Doll, A. Heßelmann, D. Kats, A. Köhn, T. Korona, D. A. Kreplin, et al. The Molpro quantum chemistry package. *J. Chem. Phys.*, 152(14):144107, 2020.

[14] M. Beseda, S. Paláček, R. Kalus, M. Benhenni, M. Yousfi, T. Leininger, and F. X. Gadéa. *Ab initio* approaches for N_2^+ and N_2^+/He ions towards modeling of the N_2^+ ion in cold helium plasma. Submitted to Comp. Theor. Chem.

[15] M. Karplus, R. N. Porter, and R. D. Sharma. Exchange reactions with activation energy. I. Simple barrier potential for (H, H_2). *J. Chem. Phys*, 43(3259):19651, November 1965.

[16] A. J. Orr-Ewing and R. N. Zare. Orientation and alignment of reaction products. *Annu. Rev. Phys. Chem.*, 45(1):315–366, October 1994.

[17] A. Chicheportiche. *Basic data of atomic and molecular helium and argon ions for the optimization of low temperature plasma jets used in the biomedical field.* PhD thesis, Université Toulouse III Paul Sabatier, 2014. In French.

[18] M. Child. *Molecular Collision Theory.* Dover Publications, Mineola, N.Y, 1996.

[19] A. Chicheportiche, M. Stachoň, M. Benhenni, F. X. Gadéa, R. Kalus, and M. Yousfi. First principles transport coefficients and reaction rates of Ar_2^+ ions in argon for cold plasma jet modeling. *J. Chem. Phys.*, 141(13):134302, oct 2014.

[20] E. A. Mason, H. O'Hara, and F. J. Smith. Mobilities of polyatomic ions in gases: core model. *J.*

Phys. B: At. Mol. Phys., 5(2):169, 1972.

[21] L. D. Landau and E. M. Lifshitz. *Quantum mechanics: non-relativistic theory*, volume 3. Elsevier, 2013.

[22] R. Johnsen, H. L. Brown, and M. A. Biondi. Ion–molecule reactions involving N_2^+, N^+, O_2^+, and O^+ ions from 300° k to $\approx 1\,\mathrm{eV}$. *J. Chem. Phys.*, 52(10):5080, May 1970.

[23] M. Yousfi, A. Hennad, M. Benhenni, O. Eichwald, and N. Merbahi. Basic data of ions in He-air mixtures for fluid modeling of low temperature plasma jets. *J. Appl. Phys.*, 112(4):043301, August 2012.

[24] R. Baranowski, B. Wagner, and M. Thachuk. Molecular dynamics study of the collision-induced rotational alignment of N_2^+ drifting in helium. *J. Chem.. Phys.*, 114(15):6662, April 2001.

[25] S. Paláček, M. Beseda, R. Kalus, M. Benhenni, M. Yousfi, T. Leininger, and F. X. Gadéa. Modeling of the N_2^+ ion in cold helium plasma III: relaxation of rotational excitations in N_2^+ in collisions with helium. under preparation.

Figures

Figure 1. Selected experimental data on the reduced mobility of N_2^+ in He at standard pressure and temperature

: diamonds Ref. [22], circles Ref. [2] (as reported in Ref. [3]), up triangles Ref. [4], and down triangles Ref. [5]. For comparison, inverse-method representations of selected experimental data are also included: full line [2], dashed line [4], and dash-dotted line [5].

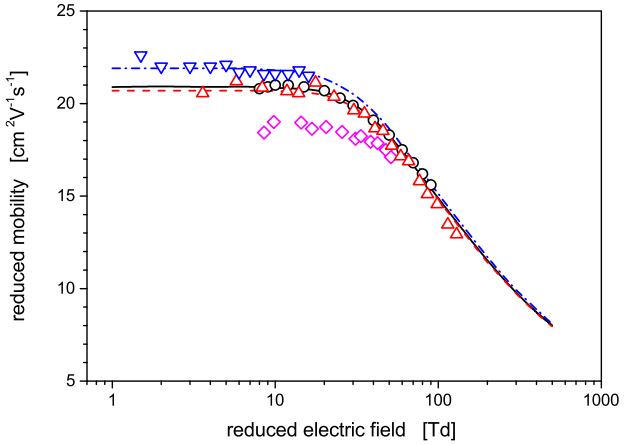

Figure 2. Reduced mobilities at standard pressure and temperature (upper panel) and longitudinal and transversal characteristic diffusion energies (lower panel, circles and triangles, respectively) of the N_2^+ ion in helium gas as calculated for the rotational-vibrational ground state of the ion (j=0,v=0) at the MCSCF/avqz(spdf) level of theory (full symbols). Inverse-method (IM) values derived from selected experimental data are also included as gray lines in the background with the line patterns used as in Fig. 1. For comparison, data resulting from an independent mobility calculation reported in the literature [24] are also shown in the upper panel (pluses). In the inset of the lower panel, a detailed view of the weak-field region is shown.

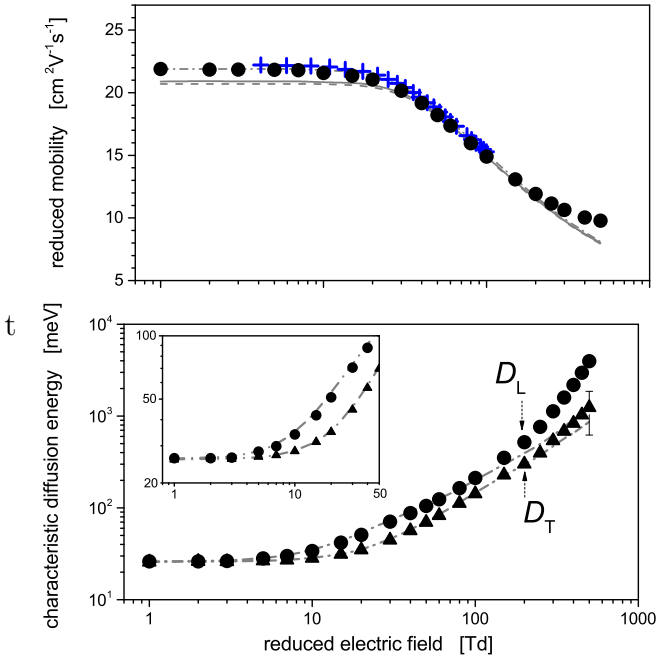

Figure 3. Distributions of center-of-mass collision energies of $N_2^+(j{=}0,v{=}0)$/He as calculated for selected values of the reduced electric field using type 1 momentum-transfer cross-sections. The distributions have been normalized so that they have the same heights in their maxima.

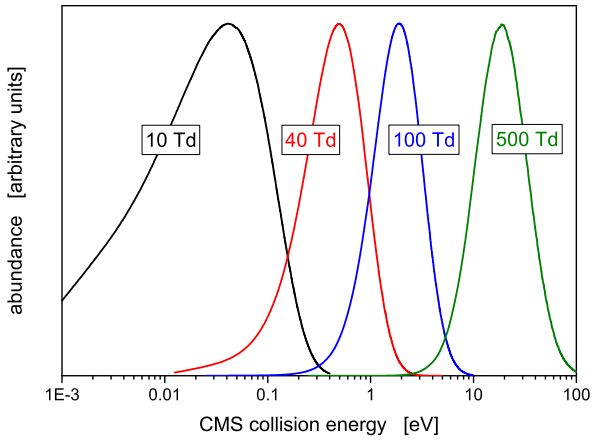

Figure 4. Reduced mobility at standard pressure and temperature (upper panel), longitudinal and transversal characteristic diffusion energies (middle panel, circles and triangles, respectively), and CID rate constants of N_2^+ ions in helium gas as calculated for selected rotational-vibrational states of the ion at the MCSCF/avqz(spdf) level: full symbols j=0,v=0, upper half-filled symbols j=0,v=1, lower half-filled symbols j=0,v=10, and open symbols j=36,v=0. Inverse-method values derived from the most recent mobility measurements [5] are also included as dash-dotted gray lines for comparison. In the insets, (absolute) deviations from the j=0,v=0 data are depicted to better see the effect of rotational-vibrational excitations in the N_2^+ ion. Note that different scales are used on the horizontal axes in the two upper panels and in the lower panel.

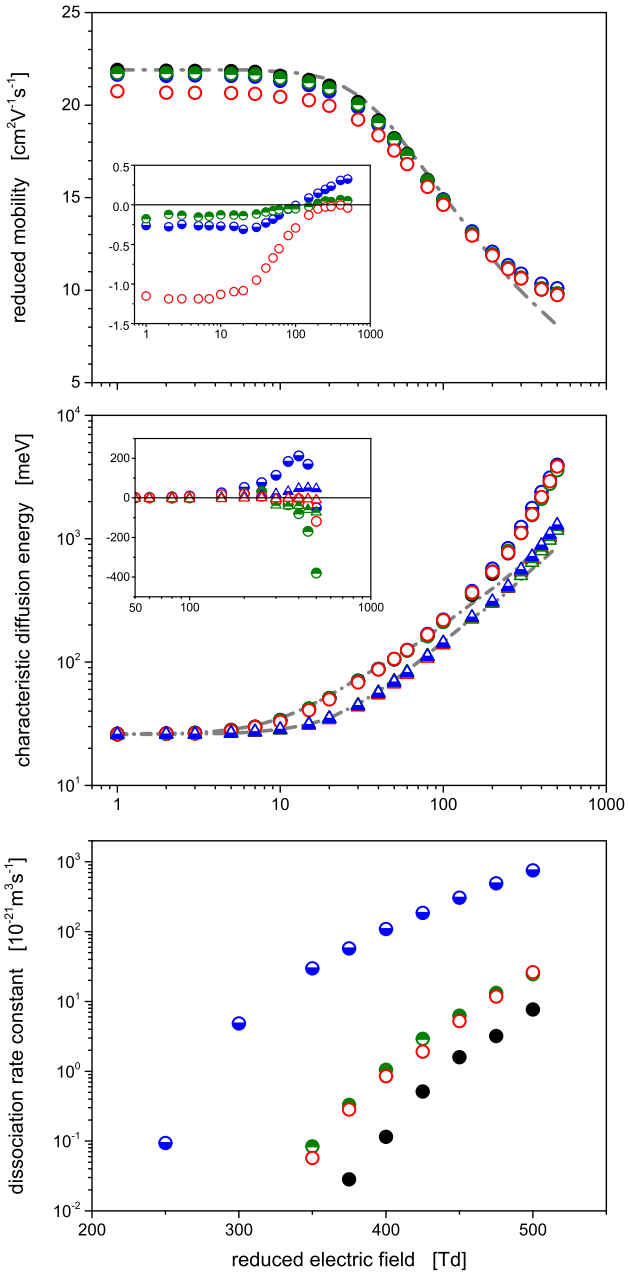

Figure 5. Deviations of N_2^+/He reduced mobilities at standard pressure and temperature

calculated using type 2 momentum-transfer cross-sections from the values obtained from type 1 cross-sections, both calculated for selected rotational-vibrational states of the N_2^+ ion at the MCSCF/avqz(spdf) level. The symbols used are the same as in Fig. 4, the connecting lines are added to guide eyes.

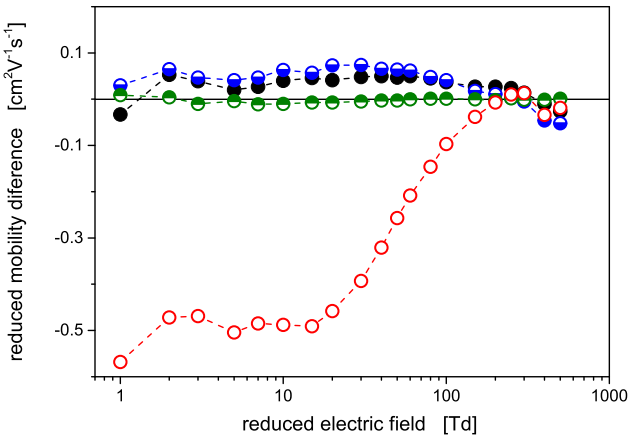

Figure 6. Comparison of N_2^+/He reduced mobilities at standard pressure and temperature

calculated using type 1 momentum-transfer cross-sections (and dissociation cross-sections) as obtained from MCSCF/avqz(spdf) calculations (full circles) and using an artificial neural network (ANN) representation of the N_2^+/He PES (pluses). In the inset, (absolute) deviations between the ANN and MCSCF/avqz(spdf) data are depicted.

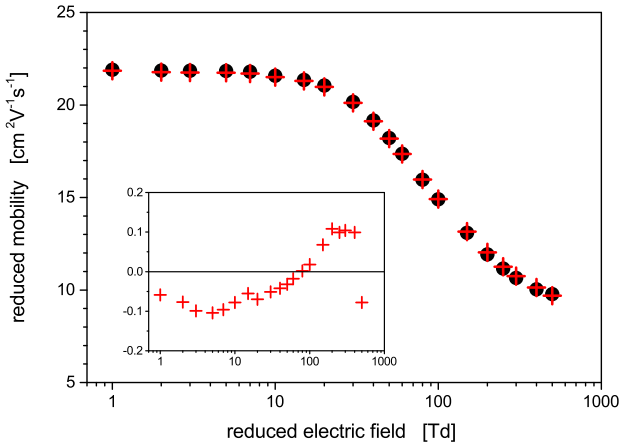

Figure 7. Comparison of N_2^+/He reduced mobilities at standard pressure and temperature

(upper panel), longitudinal and transversal characteristic diffusion energies (middle panel, circles and triangles, respectively), and CID rate constants of N_2^+ ions in helium gas calculated for rotationally-vibrationally ground-state N_2^+ ion using cross-sections obtained at the ANN level and assuming the angular momentum of the N_2^+ ion aligned perpendicularly (open circles with vertical bars, PER) and/or parallel (open circles with horizontal bars, PAR) to the collision axis, and non-aligned (full symbols). For comparison, inverse-method mobilities derived from experimental data are also depicted as grey lines in the background (with the same line patterns used as in Fig. 1). In the insets, (absolute) deviations between the values obtained from aligned angular momentum cross-sections and those obtained from non-aligned cross-sections are depicted. Note that, like in Fig 4, different scales are used on the horizontal axes in the two upper panels and in the lower panel.